Received: 18 September 2017 | Revised: 18 November 2017 | Accepted: 30 November 2017

DOI: 10.1002/hbm.23912

RESEARCH ARTICLE

WILEY

Connectivity-based parcellation of the nucleus accumbens into core and shell portions for stereotactic target localization and alterations in each NAc subdivision in mTLE patients

Xixi Zhao[1] | Ru Yang[2] | Kewan Wang[3] | Zhongping Zhang[4] | Junling Wang[1] | Xiangliang Tan[1] | Jiajun Zhang[1] | Yingjie Mei[4] | Queenie Chan[5] | Jun Xu[6] | Qianjin Feng[2] | Yikai Xu[1]

[1]Department of Medical Imaging Center, Nanfang Hospital, Southern Medical University, Guangzhou 510515, China

[2]School of Biomedical Engineering and Guangdong Provincial Key Laboratory of Medical Image Processing, Southern Medical University, Guangzhou 510515, China

[3]Department of Neurosurgery, Nanfang Hospital, Southern Medical University, Guangzhou 510515, China

[4]Philips Healthcare, Guangzhou, Guangdong 510055, China

[5]Philips Healthcare, Hong Kong, China

[6]Department of Hematology, Nanfang Hospital, Southern Medical University, Guangzhou 510515, China

Correspondence
Dr Yikai Xu, Department of Medical Imaging Center, Nanfang Hospital, Southern Medical University, Guangzhou 510515, China.
Email: yikaivip@163.com
and
Dr Qianjin Feng, School of Biomedical Engineering and Guangdong Provincial Key Laboratory of Medical Image Processing, Southern Medical University, Guangzhou 510515, China.
Email: qianjinfeng08@gmail.com

Funding information
National Key Research and Development Program of China, Grant number: 2016YFC0107104; Science and Technology Planning Project of Guangdong Province, China, Grant number: 2015B010131011

Abstract

The nucleus accumbens (NAc), an important target of deep brain stimulation for some neuropsychiatric disorders, is thought to be involved in epileptogenesis, especially the shell portion. However, little is known about the exact parcellation within the NAc, and its structural abnormalities or connections alterations of each NAc subdivision in temporal lobe epilepsy (TLE) patients. Here, we used diffusion probabilistic tractography to subdivide the NAc into core and shell portions in individual TLE patients to guide stereotactic localization of NAc shell. The structural and connection abnormalities in each NAc subdivision in the groups were then estimated. We successfully segmented the NAc in 24 of 25 controls, 14 of 16 left TLE patients, and 14 of 18 right TLE patients. Both left and right TLE patients exhibited significantly decreased fractional anisotropy (FA) and increased radial diffusivity (RD) in the shell, while there was no significant alteration in the core. Moreover, relatively distinct structural connectivity of each NAc subdivision was demonstrated. More extensive connection abnormalities were detected in the NAc shell in TLE patients. Our results indicate that neuronal degeneration and damage caused by seizure mainly exists in NAc shell and provide anatomical evidence to support the role of NAc shell in epileptogenesis. Remarkably, those NAc shell tracts with increased connectivities in TLE patients were found decreased in FA, which indicates disruption of fiber integrity. This finding suggests the regeneration of aberrant connections, a compensatory and repair process ascribed to recurrent seizures that constitutes part of the characteristic changes in the epileptic network.

KEYWORDS

connectivity-based parcellation, diffusion tensor imaging, mesial temporal lobe epilepsy, nucleus accumbens, probabilistic tractography, structural connectivity

1 | INTRODUCTION

The nucleus accumbens (NAc) is an integral part of the human brain. It is located in the basal forebrain rostral to the preoptic area. Reciprocal connections couple the nucleus accumbens with limbic structures and

Xixi Zhao, Ru Yang, and Kewan Wang contributed equally to this work.

prefrontal regions, as demonstrated by numerous anatomical and electrophysiological studies, which indicates that the NAc plays a decisive role in both functional and anatomical connectivity between the frontal and temporal lobes (Basar et al., 2010; Kandratavicius et al., 2012; Ma and Leung, 2010; O'Donnell and Grace, 1995; Postuma and Dagher, 2006). This structure has been shown to be involved in pleasure, reward, and reinforcement learning and fear, aggression, impulsivity, addiction, and the placebo effect. Therefore, it has become an important target for stereotactic deep brain stimulation in patients with some neuropsychiatric disorders that are refractory to medical treatment, such as obsessive–compulsive disorder (OCD), depression, Tourette Syndrome, and addiction (Feja, Hayn, & Koch, 2014; Francis et al., 2015; Li et al., 2013; Mavridis, Boviatsis, & Anagnostopoulou, 2011; Muller et al., 2013; Salgado and Kaplitt, 2015). Within the nucleus, the clear distinction between the shell and core subregions was defined by distinct cytoarchitectonics and connectivity patterns (Basar et al., 2010; Feja et al., 2014; Salgado and Kaplitt, 2015). These specific input–output characteristics of the two NAc subregions might represent distinctive circuits that are involved in different physiological functions (Basar et al., 2010).

A growing body of evidence has indicated that the NAc is involved in the propagation of epileptic activity in rodent models of temporal lobe seizures (Löscher, Ebert, & Lehmann, 1996; Lothman, Hatlelid, & Zorumski, 1985; Pereira de Vasconcelos, Mazarati, Wasterlain, & Nehlig, 1999), especially in the shell subdivision. Some researchers proposed that the increase in dopamine in the NAc is involved in the inhibition of seizure propagation and indicated that the NAc may be an import target for DBS to control seizures (Lothman et al., 1985). Zhou et al. showed that high frequency stimulation of the shell of the NAc significantly prolonged the latency to develop seizures, suppressed the severity of seizures and reduced the second stage and total duration of seizures in pilocarpine-induced rodent models. These findings suggest a protective role of NAc shell stimulation against seizures (Zhou Chenfei et al., 2014). Moreover, a recent clinical study provided initial evidence for the safety and feasibility of the chronic electrical stimulation of the NAc in patients with intractable partial epilepsy, as indicated by largely unchanged neurocognitive function and psychiatric comorbidity (Schmitt et al., 2014). Thus far, many studies have used anatomical MRI and fMRI to study the morphological, functional, and structural connections of the whole NAc in animal models, postmortem samples, and healthy people. However, little is known about the exact parcellation within the NAc in individual TLE patients, furthermore its microstructural abnormalities or the connection alterations of each NAc subdivision remain unclear, which may underlie the pathophysiological mechanism of seizure generation and propagation in TLE patients.

Connectivity-based parcellation divides a region of interest into distinct subregions, capitalizing on the distinct connections of each area derived from diffusion magnetic resonance imaging or resting-state functional connectivity (Eickhoff, Thirion, Varoquaux, & Bzdok, 2015). Diffusion tensor tractography can capture anatomical connectivity between brain regions in vivo, which is evidently closest to the underlying cytoarchitectonics derived from postmortem data (Klein et al., 2007; Seehaus et al., 2013). Therefore, it has been used extensively to parcellate brain regions based on their structural connectivity profiles (Barron, Tandon, Lancaster, & Fox, 2014; Chowdhury, Lambert, Dolan, & Duzel, 2013; Liu et al., 2013; Saygin, Osher, Augustinack, Fischl, & Gabrieli, 2011; Tomassini et al., 2007). The purpose of this study was to parcel the nucleus accumbens into core and shell portions using DTI probabilistic tractography in individual mesial temporal lobe epilepsy (mTLE) patients to guide NAc shell stereotactic target localization and to investigate structural abnormalities and connection alterations of each NAc subdivision in mTLE patients.

2 | MATERIALS AND METHODS

2.1 | Subjects

This study was conducted in the Department of Diagnostic Imaging Center, Nanfang Hospital, Guangzhou, China, from May 2013 to August 2015. Forty consecutive mTLE patients and 25 healthy controls matched for age, gender, and handedness participated in this study. Patients diagnosed with mesial temporal lobe epilepsy and admitted to the indoor Department of Neurology were enrolled in the study. All patients underwent a comprehensive clinical evaluation that included a careful interview, neurological examination, neuropsychological assessment, and neurophysiological monitoring according to the epilepsy classifications of the International League Against Epilepsy (ILAE) (Berg et al., 2010). Inclusion criteria for this study were as follows: (a) seizure types and epileptic syndromes of mTLE; (b) interictal and ictal electroencephalogram (EEG) or/and video-EEG evaluations that indicated the presence of epileptiform abnormalities over temporal or frontotemporal regions; (c) no foreign tissue lesions; and (d) MRI manifestation of unilateral hippocampal sclerosis subsequently confirmed by postsurgical histopathology. Finally, a total of 34 patients with unilateral mTLE were included in this study (16 patients with left mTLE, 6 females, mean age 23.9 ± 11.1 years; and 18 patients with right mTLE, four females, mean age 28.3 ± 8.4 years). There was no statistically significant difference in age in the right mTLE ($n = 18$), left mTLE ($n = 16$), and control ($n = 24$) groups. Similarly, there was no significant difference in disease duration between the right and left mTLE groups. The study protocol was approved by the Research Ethics Committee of Nanfang Hospital of the Southern Medical University. Written informed consent was obtained from each subject prior to this study. Table 1 lists the demographic information for all the patients and the controls.

2.2 | Image acquisition

All MRI imaging was performed on a Philips Achieva 3 T MRI scanner (Philips Healthcare, Inc., Best, The Netherlands) equipped with an 8-channel head coil. The DTI data were collected along the anterior commissure/posterior commissure line using a single-shot spin-echo Echo-Plannar Imaging (EPI) sequence with the following parameters: TR = 7542 ms, TE = 86 ms, FOV = 224×224 mm^2, matrix size 112×112, voxel size = $2 \times 2 \times 2$ mm^3, and 70 axial slices with no interslice gap to cover the whole brain. We applied the diffusion-weighted

TABLE 1 Clinical information and characteristics of mTLE patients and controls

	Control	LTLE	RTLE	p value
N (female)	25 (13)	16 (6)	18 (4)	0.141[a]
Age (m ± std, years)	25.56 ± 2.53	23.9 ± 11.1	28.3 ± 8.4	0.230[b]
Duration of epilepsy (m ± std, years)		8.8 ± 5.4	9.4 ± 6.9	0.782[c]
Age of onset (m ± std, years)		15.8 ± 11.6	19.2 ± 10.7	0.389[c]

[a]Chi-square test.
[b]One-way ANOVA.
[c]Two-sample *t* test.

gradients along 32 directions with b = 1000 s/mm^2. In addition, we acquired high-resolution 3D sagittal T1-weighted images with the following parameters: TR = 8.3 ms, TE = 3.9 ms, FOV = 240 mm × 240 mm, matrix size = 240 × 240, FA = 13°, voxel size = 1 mm × 1 mm × 1 mm, and 150 sagittal slices without interslice gap.

During the acquisition, subjects were placed in a supine position in the gantry of the scanner with foam padding to limit head movement and ear plugs to reduce the impact of acoustic noise.

2.3 | Data preprocessing

Preprocessing was performed with tools from the FMRIB Software Library (FSL) (www.fmrib.ox.ac.uk/fsl). For each subject, we skull-stripped the diffusion-weighted and T1-weighted images. All diffusion-weighted images were corrected for eddy current distortion and head motion by the Diffusion Toolbox of Functional MRI of the Brain (FMRIB). The preprocessed DTI data were fit to a diffusion tensor model to generate fractional anisotropy (FA), mean diffusivity (MD), and three eigenvectors maps. Skull-stripped T1-weighted images were coregistered to the subject's non-diffusion-weighted images. The T1 images in diffusion space were then transformed to the Montreal Neurological Institute (MNI) space. The transformation matrices from any of the three spaces into another space were also derived for the following analysis.

2.4 | DTI connectivity-based parcellation of the NAc in individuals

The DTI connectivity-based parcellation was performed using previously described procedures (Baliki et al., 2013) and the flow diagram is shown in Figure 1. For each subject, T1-weighted scans were processed using FIRST (fMRIB Integrated Registration and Segmentation Tool) to localize the NAc in both the left and right hemispheres. Subject-specific NAc maps were then linearly registered to the individual native diffusion space. Whole-brain probabilistic tractography was performed in native diffusion space using the PROBTRACKX to estimate the connections between each NAc seed voxel and any target voxel in the whole brain, which were defined as the number of tracts arriving at the target site. A total of 5000 samples were automatically drawn to build the a posteriori distribution of the connectivity distribution. The number of samples 5000 is default setting of PROBTRACKX. With this number of samples, they are confident that convergence is reached (https://fsl.fmrib.ox.ac.uk/fsl/fslwiki/FDT/UserGuide#PROBTRACKX). To reduce the false-positive connections, we thresholded the path distribution estimates from ProbTrack using a connection probability of $p < .01$ (50 of 5000 samples).

The connectivity matrix A between NAc seed voxels and target voxels was derived, and used to generate a symmetric cross-correlation matrix $B=AA^T$, of dimensions number of seeds × number of seeds. The cross-correlation matrix was then fed into a k-means clustering algorithm to group together the seed voxels that share similar connection profiles with the rest of the brain. This automated classification produced an individual parcellation of the NAc into two clusters. Then, core and shell subdivisions were identified for each subject by the location and shape as described in previous anatomical studies (Basar et al., 2010; Voorn, Brady, Berendse, & Richfield, 1996).

To validate the reproducibility of DTI connectivity-based parcellation method, we also conducted our parcellation scheme. We scanned DTI twice on one healthy subject and conducted our parcellation scheme on left NAc. Subdivisions were then transformed into the same T1 space for comparison. Reproducibility between scans was quantified as the conditional probability that a voxel classified as belonging to a particular region in scan01 would receive the same classification in scan02 as in $P_{scan01} = |subdivision_{scan01} \cap subdivision_{scan02}| / |subdivision_{scan01}|$, as previously described (Klein et al., 2007). For each subdivision, conditional probability was calculated twice, crossing over the subdivisions between runs. The reproducibility was finally obtained by averaging the conditional probabilities of two scans.

2.5 | Measurement of diffusion parameters and volume of the NAc subregions

For each subject, the corresponding diffusion parameters were extracted from NAc subdivisions in individual DTI space and included fractional anisotropy (FA), mean diffusivity (MD), radial diffusivity (RD), axial diffusivity (AD), and three eigenvalues, corresponding to eigenvectors oriented along three orthogonal directions (λ_1, λ_2, and λ_3). Statistical analysis was performed with SPSS 20.0 (IBM SPSS, Chicago, IL). FA, MD, AD, and RD values and three eigenvalues in left and right mTLE groups were compared with those in the control group for each NAc subdivision, using repeated-measures ANOVA to test the effects of hemispheres (2 levels), subregions (2 levels), and groups (2 levels). Post hoc pairwise comparisons with Bonferroni corrections for multiple comparisons were used to discriminate the diffusion parameters of

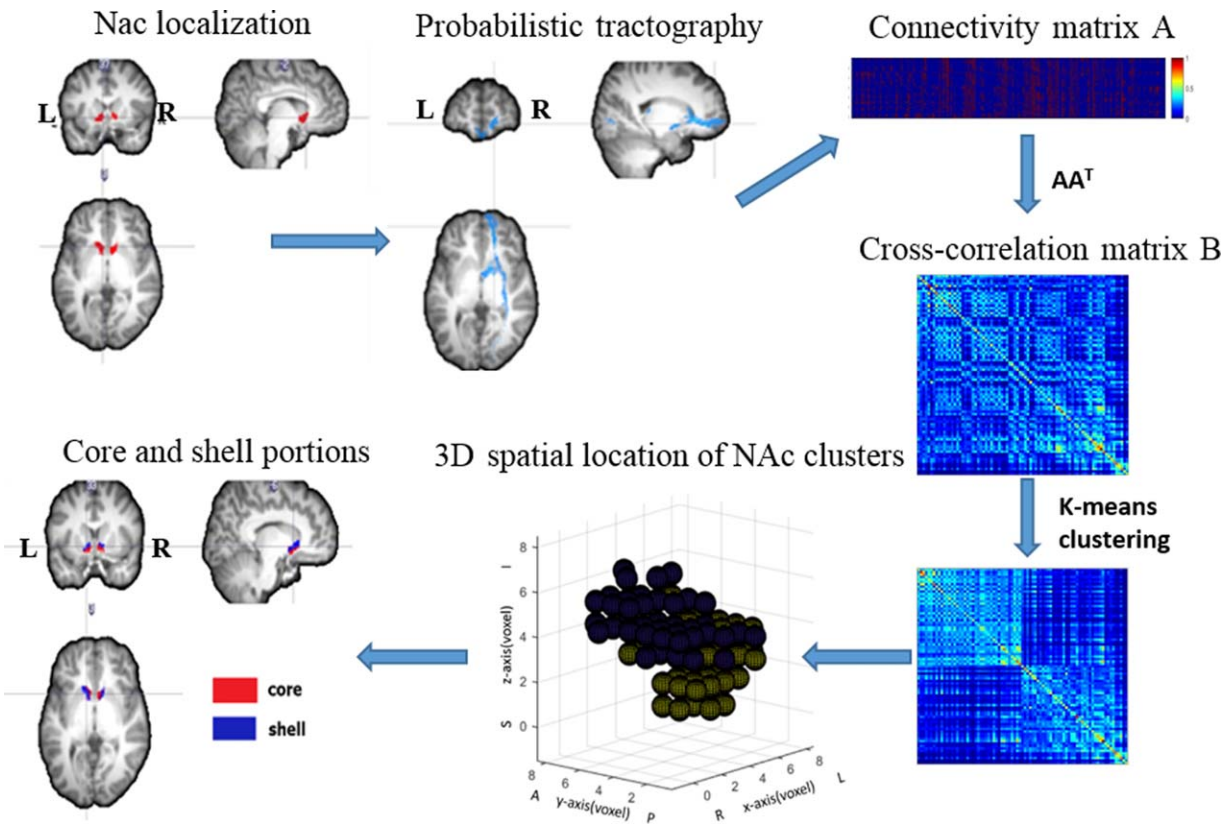

FIGURE 1 The flow diagram of DTI connectivity-based parcellation procedures. The subject-specific NAc masks were generated. Whole-brain probabilistic tractography was performed on each NAc seed voxel. The connectivity matrix A between NAc seed voxels and voxels of whole brain was then derived. Symmetric cross-correlation matrix B=AA^T; B was then fed into k-means clustering algorithm to divide NAc into two clusters. Finally, core and shell subdivisions were identified for each subject according to their location and shape [Color figure can be viewed at wileyonlinelibrary.com]

each subdivision of each hemisphere in the three groups. We also assessed group differences of volumes in both the core and shell using two-sample *t* tests.

2.6 | Anatomical connectivity patterns of the NAc subregions

To investigate different anatomical connection patterns of each NAc subregion in the three groups, the subject-specific NAc subdivisions were then transformed into standard MNI space to generate group-averaged subdivisions. Group-averaged subdivisions were determined by overlapping all subjects' subdivisions. To maintain a similar size for the same subdivisions in the bilateral NAc and to ensure the maximum size for subdivisions without overlap, discrete and spatially contiguous subdivisions with no overlap were designed as follows. The group-level subdivisions of the left core, left shell, right core, and right shell were determined as regions of 45%, 45%, 40%, and 40% overlap, respectively, across individual subjects' parcellation of the NAc. This step ensures that a consistent seed ROI was obtained, mitigating volume and shape differences among individuals. The group-averaged NAc subdivisions were then used as ROIs to define probabilistic connections with predefined ipsilateral target ROIs.

We evaluated the probabilistic connections between each group-averaged NAc subdivision and 16 predefined target regions in the standard space using the PROBTRACKX for every subject. In accordance with previous tract tracing (Baliki et al., 2013; Lucas-Neto et al., 2015) and anatomical studies (Basar et al., 2010; Haber, 2011; Haber and Knutson, 2010), sixteen target regions in the same hemisphere were chosen (Figure 4b). These target regions were extracted from the Harvard–Juliet atlas and included the amygdala (AMY), caudate (CAU), anterior cingulate cortex (ACC), posterior cingulate cortex (PCC), orbital frontal cortex (OFC), frontal pole (FP), hippocampus (HIP), insula (INS), globus pallidus (GP), paracingulate gyrus (PCG), anterior-parahippocampal gyrus (Ante-PHG), posterior-parahippocampal gyrus (Post-PHG), putamen (PUT), subcallosal cortex (SCC), thalamus (THA), and temporal pole (TP).

The probability of structural connectivity from the seed to each target was defined as the number of fibers passing through the target from the seed divided by the number of fibers that were sampled in the seed (5000 × number of voxels in the seed). Connection probabilities were then divided by the size of the target region to produce normalized connection probabilities adjusted for the volume of the target region.

For the control group, a three-way repeated-measures ANOVA was performed to test the main effects of hemispheres, NAc subdivisions and target regions on the normalized connection probabilities.

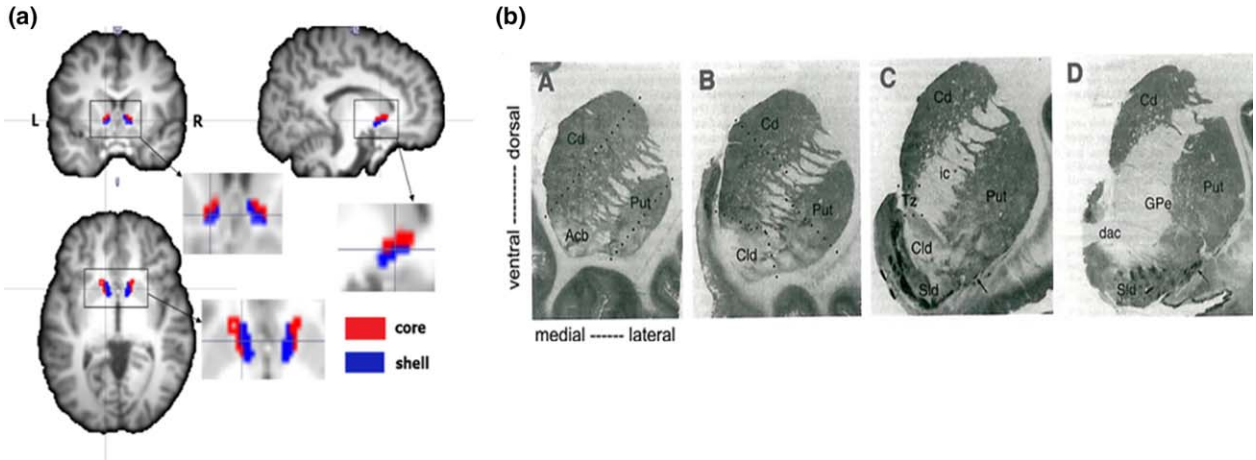

FIGURE 2 (a) NAc connectivity-based parcellation results in one subject. (b) A series of frontal sections through the striatum from a single human brain illustrating the pattern of [^{3}H]DAMGO binding at four rostrocaudal levels. Images taken from Voorn et al. (1996), in which they identify the Core-like division (Cld) and shell-like division (Sld) of the accumbens (Acb). The location and shape of the core (red) and shell (blue) subdivisions (a) approximate cytoarchitecturally identified Cld and Sld (b), respectively [Color figure can be viewed at wileyonlinelibrary.com]

Pairwise comparisons with Bonferroni corrections for multiple comparisons were used to discriminate the connectivity probabilities between each NAc subdivision to all targets.

To quantify the differences in anatomical connections of each NAc subregion in the healthy controls and TLE groups, the connection probabilities with the 16 target regions were entered into an NAc subregions (2 levels) × target regions (16 levels) × hemispheres (2 levels) repeated-measures ANOVA. Post hoc pairwise *t* tests with Bonferroni corrections for multiple comparisons were performed to visualize the anatomical connection probabilities differences in each subdivision in the healthy control and TLE groups.

2.7 | Diffusion parameters in group-averaged white matter tracts connecting ROIs with each subdivision of the NAc

After tractography, the tracts from each NAc subdivision to any targets were then overlapped onto standard space across all subjects to generate common pathways. After thresholding and visual inspection, only the continuous common pathways were retained. The common pathways were then mapped back to the diffusion space, from which the mean FA and MD values were extracted. Two-sample *t* tests were performed to assess the group differences on each group common tract.

3 | RESULTS

3.1 | Connectivity-based parcellation and identification of two spatially discrete subdivisions of the NAc in individuals

Using DTI connectivity-based parcellation, the individual NAc regions were subdivided into two portions based on clustering the similar connection profiles of whole-brain structural connectivity in subject-specific diffusion space. The parcellation of each NAc into two discrete,

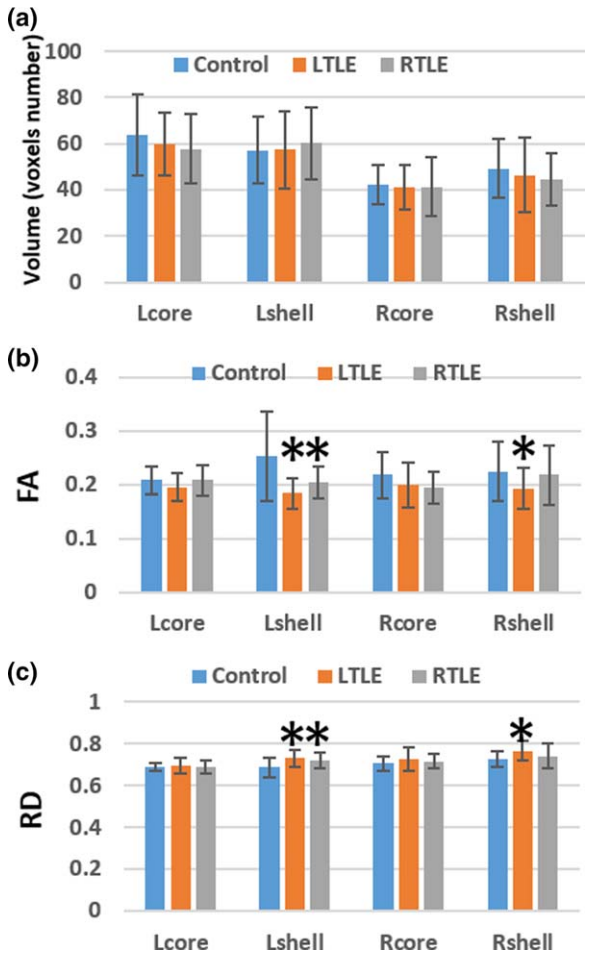

FIGURE 3 Comparison of the volumes, FA, and RD values of each subdivision of NAc between control and mesial temporal lobe epilepsy groups. Volume is represented by voxels number of subdivisions in individual DTI space. RD, radial diffusivity; Units for radial diffusivity = $\times 10^{-3}$ mm^2/s. * denotes a significant difference ($p < .05$) between control and mTLE groups [Color figure can be viewed at wileyonlinelibrary.com]

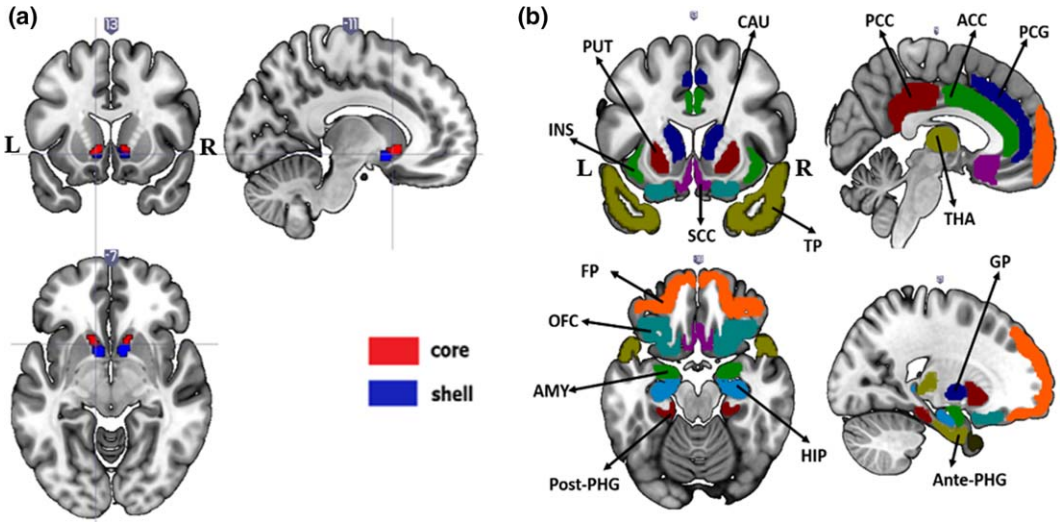

FIGURE 4 (a) Group-averaged subdivisions of the NAc and (b) the targets of interest employed in this study overlaid onto a T_1-weighted template in standard space. All target regions were extracted from the Harvard–Juliet atlas, which included the AMYG, CAUD, ACC, PCC, OFC, FP, HIP, INS, GP, PCG, Ante-PHG, Post-PHG, PUTA, SCC, THAL, and TP [Color figure can be viewed at wileyonlinelibrary.com]

spatially contiguous subdivisions was successful in 24 of 25 controls, 14 of 16 left mTLE patients, and 14 of 18 right mTLE patients. One control, 2 left mTLE patients and 4 right mTLE patients failed to do the parcellation because some clusters were spatial discontinuous in these subjects. In each of these subjects, the NAc was divided into a medial–caudal portion and a lateral-rostral one. The location and shape of the two portions approximately matched the cytoarchitecturally identified NAc core and shell in postmortem human tissue (Voorn et al., 1996). Based on this similarity, we identified the medial–caudal portion as the shell and the lateral–rostral portion as the core of the NAc. Representative individual parcellation is shown in Figure 2.

The reproducibility of our connectivity-based parcellation method were 82.46% for core and 81.74% for shell. NAc subdivisions from two scans were transformed into the same T1 space for comparison, as shown in Supporting Information, Figure S1.

3.2 | Comparisons of diffusion parameters and volume of each NAc subdivision in mTLE patients and healthy controls

In general, the volume of each NAc subdivision in the left and right TLE patients was not different from those of the controls (Figure 3a and Supporting Information, Table I). Compared to the control group, left mTLE group showed significant group differences in FA and RD values. However, the MD and AD values did not exhibit significant group differences. Concerning the FA values, there was a significant main effect in the subdivision × group interaction ($F = 8.574$, $p = .006$), but there was no significant main effect in hemisphere ($F = 1.091$, $p = .303$) or subdivision ($F = 2.384$, $p = .131$). The RD values exhibited significant main effects in hemisphere ($F = 45.066$, $p < .0001$), subdivision ($F = 19.441$, $p < .0001$), and subdivision × group interaction ($F = 7.723$, $p = .009$) when the left mTLE group was compared with controls. The left mTLE group showed significantly decreased FA and elevated RD in the bilateral shell portion after correcting for multiple comparisons, but the core portion did not exhibit a significant difference.

In the right mTLE, there was a significant group difference only in λ_3 values (the third eigenvalue). However, the interaction of group by subdivision × hemisphere was significant in terms of FA values. The group differences in diffusion parameters were not significant. Nor were the main effects of within-subject factors and their interactions. After correcting for multiple comparisons, the right mTLE group exhibited decreased FA values and increased RD and λ_3 values in the left shell. However, the right shell and bilateral core portions did not yield any significant differences (Figure 3b,c and Supporting Information, Tables II–V).

3.3 | Structural connectivity patterns of each group-averaged NAc subdivision in healthy controls

Group-averaged subdivisions were determined by overlapping all subjects' subdivisions (Figure 4a). The voxel numbers of the subdivisions described above were 31, 31, 29, and 30. Using DTI probabilistic tractography, fiber pathways of the two NAc subregions were delineated. The group averaged white matter tracts identified for each part of the NAc presented relatively distinct pathways in healthy controls.

In healthy controls, there were significant main effects in subdivision ($F = 156.857$, $p < .0001$), target ($F = 418.921$, $p < .0001$) and subdivision × target interaction ($F = 379.831$, $p < .0001$), but there was no significant main effect in hemispheres ($F = 0.357$, $p = .556$). Significant differences in the core and shell connectivity to each target region were then determined via a post hoc analysis. The core exhibited higher structural connectivity to the caudate, FP, and THAL. In contrast, the shell showed higher connectivity to the AMYG, PCC, OFC, parahippocampus, putamen, SCC, and TP. Both NAc subdivisions showed similar connectivity strength to ACC, HIP,

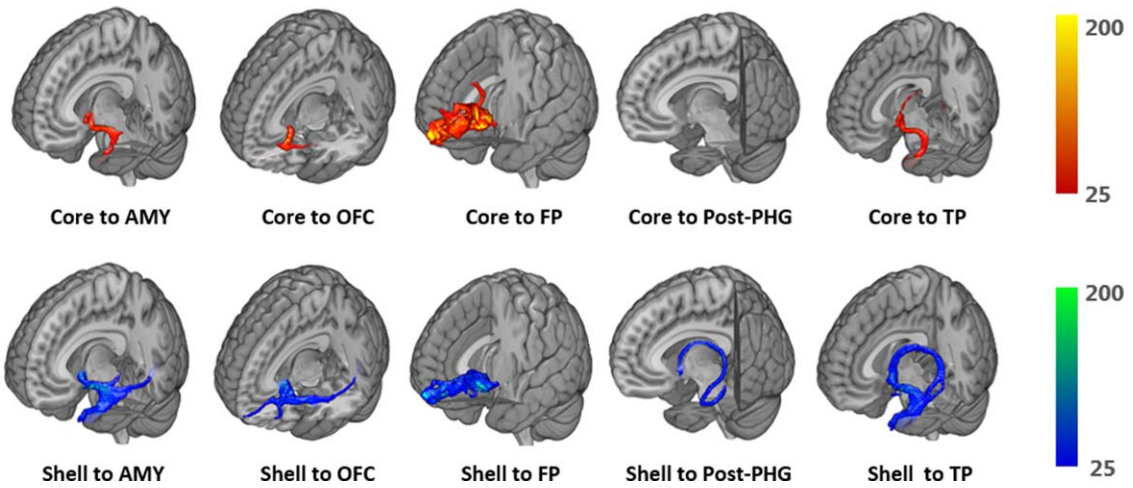

FIGURE 5 Probabilistic tractography for several representative tracts in the left hemisphere from one single subject. Voxels are color coded from 25 to 200 (tracts from core are red to yellow, tracts from shell are blue to green) represented the number of fibers passing through the voxel. Corresponding targets from left to right are AMY, OFC, FP, Post-PHG, and TP [Color figure can be viewed at wileyonlinelibrary.com]

INS, GP, PCG, and Post-PHG (Figures 5 and 6a and Supporting Information, Table VI).

3.4 | Quantitative comparisons of structural connections of each NAc subregion in healthy controls and TLE groups

To quantify the differences in anatomical connections of each NAc subregion in the healthy control and TLE groups, normalized connection probabilities were entered into an NAc subregions (2 levels) × target regions (16 levels) × hemispheres (2 levels) repeated-measures ANOVA. Post hoc comparisons were performed to visualize the anatomical connection probabilities differences in each subdivision in the healthy control and TLE groups.

There were no significant between-group differences ($F = 3.115$, $p = .085$) or hemisphere main effect ($F = 0.434$, $p = .514$) when comparing the left mTLE group with controls; however, the subdivision ($F = 191.338$, $p < .0001$) and target ($F = 1362.169$, $p < .0001$) main effect and their interaction of group ($F = 3.035$, $p = .024$) were significant. The results of ANOVAs for group effects on each connectivity between NAc subdivisions and 16 target regions were corrected for multiple comparisons and are summarized in Figure 6b,c and Supporting Information, Tables VII–X. Concerning the left hemispheric pathways, the left mTLE group showed significantly increased connectivity in the ACC-core and decreased THAL-core connectivity. However, the shell portion exhibited a remarkable increase in ACC-shell, OFC-shell, PCG-shell, and SCC-shell relative connectivity and a significant decrease in HIP-shell and THAL-shell relative connectivity. In the right hemisphere, the core portion did not exhibit any significant group differences, while the right shell showed a significant increase in SCC-shell connectivity.

In the right mTLE, there were no significant between-group differences ($F = 1.913$, $p = .174$) compared with controls. Although the main effects of hemisphere ($F = 8.479$, $p = .006$), subdivision ($F = 228.341$, $p < .0001$), target ($F = 1533.980$, $p < .0001$) and their interactions (28.079, $p < .0001$) were significant, the interaction of group by subdivision × target was not significant. Corrected for multiple comparisons, the right mTLE group exhibited significantly lower connectivity in the left FP-shell and right anterior PHG-core and an elevated connectivity in the right SCC-shell. However, the left core portion in the right mTLE group did not yield any significant group differences. In general, mTLE patients presented more extensive connection alterations in the shell than the core portion of the NAc (Figure 6b,c).

3.5 | Comparisons of diffusion parameters in group-averaged white matter tracts that connect ROIs with each subdivision of the NAc in the groups

The resulting group-averaged tracts and significant differences in diffusion parameters in these tracts that connect ROIs with each subdivision of the NAc in the groups are illustrated in Figure 7 and Supporting Information, Tables XI–XIV. Although not all significant, elevated MD values and reduced FA values were generally found in TLE patients. The MD value was significantly increased in tracts that connected the left amygdala, caudate, OFC, FP, Hipp, INS, GP, putamen, and TP with the left NAc core portion and in tracts that connected the left amygdala, FP, Hipp, INS, GP, putamen, and TP with the left shell of the NAc in left TLE patients. In the right hemisphere, left TLE patients presented increased MD values in tracts that connected the amygdala, OFC, and FP with the core and in tracts that connected the amygdala, INS, and GP with the shell portion. However, right TLE patients showed increased MD values in tracts that connected the left amygdala, caudate, FP, putamen, and TP with the left core and in tracts that connected the amygdala, FP, putamen, SCC, and TP with the left shell. Additionally, elevated MD values were detected in the tracts projecting form right caudate, OFC, FP, INS, putamen, and TP to the right core

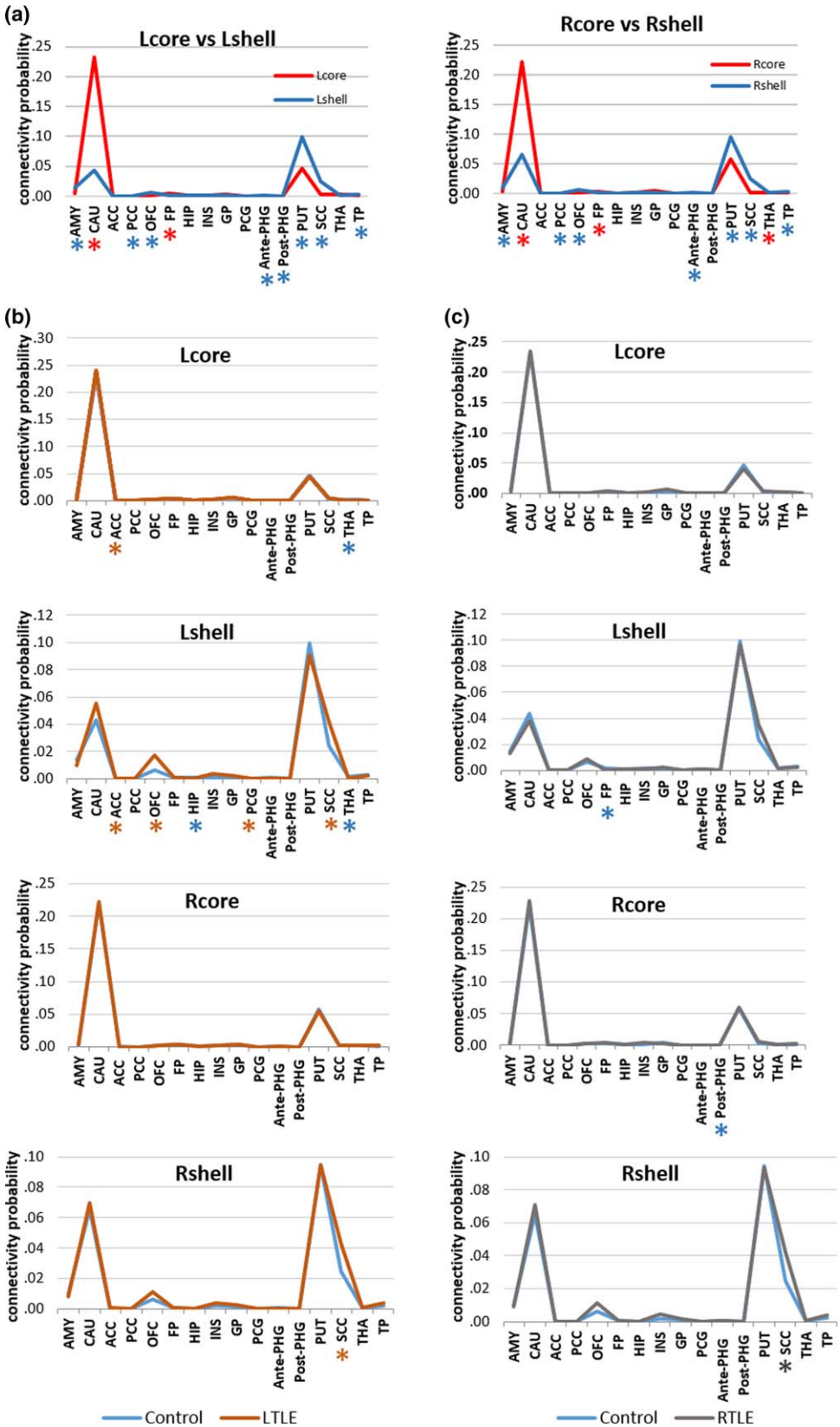

FIGURE 6 (a) Structural connectivity probabilities differences between the NAc subdivisions in healthy controls. (b,c) Structural connectivity probabilities differences in each NAc subdivision between healthy control and mTLE groups. The values indicate relative connection probabilities of white matter tracts based on DTI tractography for the shell and core to the targets. * denotes a significant greater connectivity probability of the subdivision or group in corresponding color [Color figure can be viewed at wileyonlinelibrary.com]

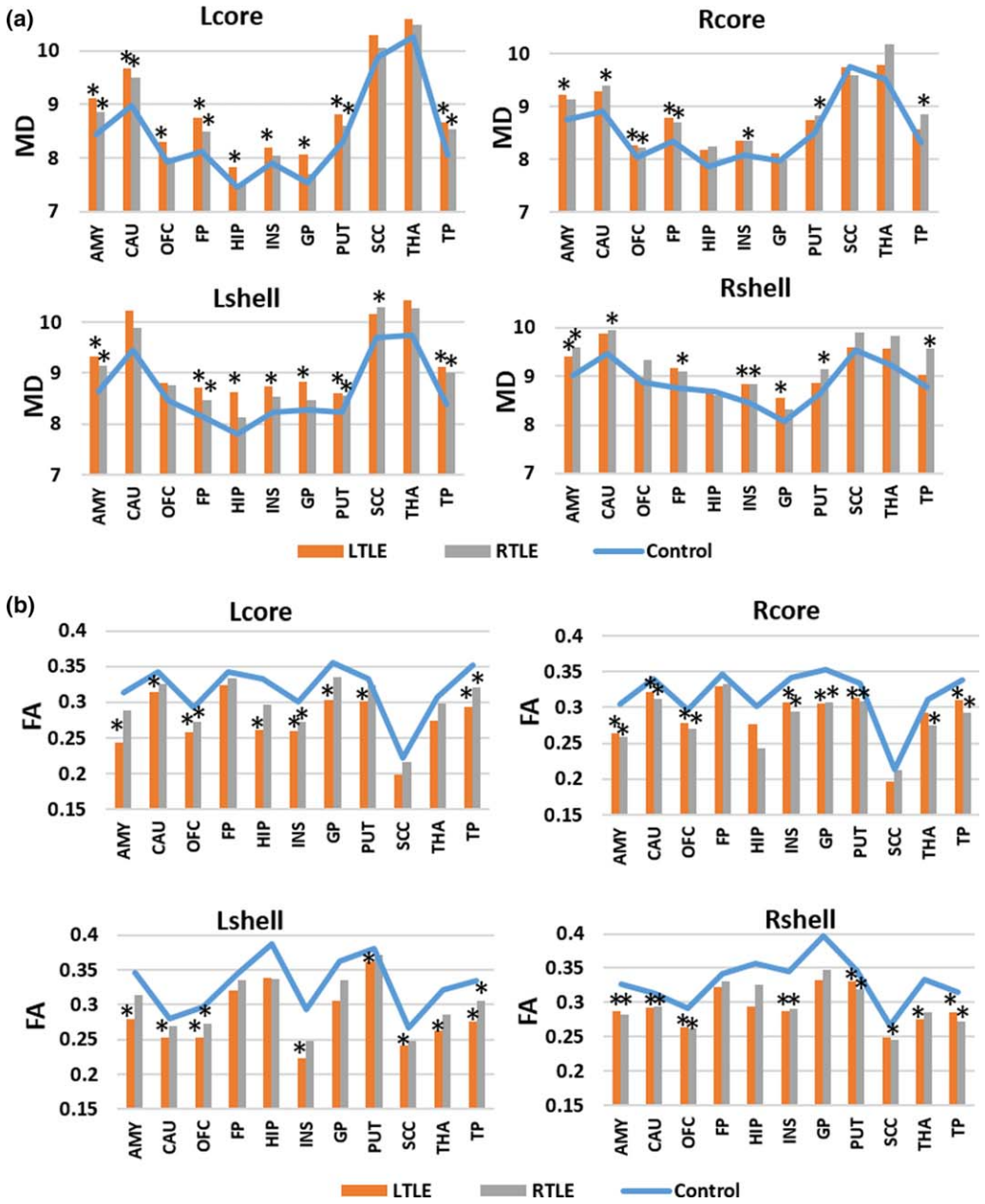

FIGURE 7 Comparison of MD and FA values in group averaged white matter tracts that connect ROIs with NAc subdivisions between control and TLE groups. * denotes a significant between-group difference of $p < .05$ [Color figure can be viewed at wileyonlinelibrary.com]

and projecting from right amygdala, caudate, FP, INS, putamen, and TP to the shell in right TLE patients.

Left TLE patients exhibited significantly reduced FA values in tracts that connected the amygdala, caudate, OFC, Hipp, INS, GP, putamen, and TP with the core, and in tracts that connected the amygdala, caudate, OFC, INS, putamen, SCC, THAL, and TP with the shell in the left hemisphere. In the right hemisphere, left TLE patients presented with decreased FA values in tracts that connected the amygdala, caudate, OFC, INS, GP, putamen, and TP with the core, and in tracts that connected the amygdala, caudate, OFC, INS, putamen, THAL, and TP with the shell portion. The right TLE patients showed decreased FA values in the left OFC-core, INS-core, and TP-core tracts and in the left OFC-shell and TP-shell tracts. However, in right TLE patients, decreased FA were detected in these tracts projecting from right amygdala, caudate, OFC, INS, GP, putamen, THAL and TP to the core, and connecting right amygdala, caudate, OFC, INS, putamen, SCC, and TP with the shell.

4 | DISCUSSION

In this study, we parceled the nucleus accumbens into core and shell portions using DTI probabilistic tractography in individual mTLE patients and controls, constructed structural connectivities of each NAc subdivision for all participants, and then compared the structural abnormalities and connection alterations in each NAc subdivision

among TLE patient groups and controls. The main findings were as follows: (a) We successfully segmented the nucleus accumbens into two different sectors in 24 of 25 controls, 14 of 16 left mTLE patients, and 14 of 18 right mTLE patients, on the basis of their anatomical connection patterns. (b) Compared to controls, mTLE patients presented significant alterations in the shell portion rather than the core. (c) We elucidated the anatomical connectivity patterns of the human NAc at the subregional level and demonstrated relatively distinct structural connectivity of each NAc subregion. The core exhibited higher structural connectivity to the caudate, FP, and THAL, while the shell showed higher connectivity to the AMYG, PCC, OFC, parahippocampus, putamen, SCC, and TP. (d) More extensive connection abnormalities were found in the NAc shell when the mTLE groups were compared with controls. Remarkably, neuronal fiber loss and paradoxical increased connectivities were found in the SCC-shell and OFC-shell tracts.

4.1 | Subdivisions of the NAc

As noted by previous researches, the cytoarchitectonic and chemoarchitectonic features of NAc shell and core subregions are quite distinct. Cytoarchitectonically the core is very homogeneous, which has a lower concentration of opiate receptors and a higher concentration of calcium-binding proteins. However, the shell exhibits strong inhomogeneities in the distribution of various neurochemical substances and neurotransmitter receptors, among which mu-opioid receptors and dopamine receptors. (Basar et al., 2010; Feja et al., 2014; Rigoard et al., 2011; Salgado and Kaplitt, 2015; Voorn, Brady, Schotte, Berendse, & Richfield, 1994).

Previous reports examined the in vivo segmentation of the healthy human NAc using probabilistic tractography (Baliki et al., 2013; Lucas-Neto et al., 2015). To our knowledge, we are the first to parcellate the nucleus accumbens of individual mTLE patients into core and shell portions using DTI probabilistic tractography in vivo. The exact stereotactic anatomy of the core and shell portions of the NAc in individual epilepsy patients would help neurosurgeons to perform deep brain stimulation (DBS) of the NAc shell to suppress seizure propagation. Using DTI connectivity-based parcellation, each NAc was successfully parcellated into two subdivisions in a total of 24/25 controls, 14/17 left TLE patients, and 18/23 right TLE patients in subject-specific diffusion space. The location and shape of the two portions approximately matched the cytoarchitecturally identified NAc core and shell in postmortem human tissue (Voorn et al., 1996). Based on this correspondence, we identified the medial-caudal portion as the shell and the lateral-rostral portion as core of the NAc.

4.2 | Differences in diffusion parameters in each NAc subdivision in the mTLE patients and controls

Most prior studies using DTI reveal changes preferentially in white matter structures, which reflect axonal number, membrane circumference, and myelin thickness information in white matter. However, some previous researches detected changes in gray matter by DTI in patients and animal models of epilepsy. Parekh et al. (2010) found changes in FA in the hippocampus, amygdala, entorhinal cortex, piriform cortex, and thalamus in a limbic status epilepticus model of epileptogenesis. Wang et al. (2017) investigated decreases and increases in FA in regions such as the entorhinal-hippocampal area, amygdala, thalamus, striatum, accumbens, and neocortex in methionine sulfoximine-infused rats as model of human MTLE. Peng et al. (2014) observed altered diffusion parameters of subcortical gray matter in patients with MRI-negative cortical epilepsy using DTI, and reported the decrease in FA values in the bilateral nucleus accumbens in epilepsy patients for the first time. The decreases in FA using DTI are known to occur in gray matter areas during cerebral ischemia and sustained seizures. Such decreases in FA are thought to reflect blood–brain barrier disruption with cytotoxic edema and contraction of the extracellular space volume (Wang et al., 2017).

Our results revealed that left mTLE patients exhibited decreased FA and increased RD values in the shell portion of the bilateral NAc, and no significant alterations were observed in the core. However, the right mTLE patients showed decreased FA and increased RD values only in the left shell portion. This finding may indicate that neuronal degeneration and damage caused by seizures exist mainly within shell portions.

As a central relay structure between limbic and mesolimbic dopaminergic structures, the mediodorsal thalamus and the prefrontal cortex, the nucleus accumbens is well known to be involved in the pathophysiology of some psychiatric disorders, such as treatment-resistant depression and OCD (Basar et al., 2010; Bewernick et al., 2010; Boccardi et al., 2013; Rigoard et al., 2011; Sturm et al., 2003). However, studies have recently focused on the role of the nucleus accumbens in epileptogenesis (Löscher et al., 1996; Lothman et al., 1985; Pereira de Vasconcelos et al., 1999), especially on its shell subdivision. Using lithium pilocarpine-induced status epilepticus as a model of human TLE, Scholl, Dudek, & Ekstrand (2013) observed neuronal degeneration in several distinct areas outside hippocampal regions, including in the accumbens shell, which suggested a possible role of the accumbens shell in epileptogenesis and supports our findings. Ma, Boyce, and Leung (2010) found that mu opioid receptors in the nucleus accumbens mediate immediate postictal decrease in locomotion after an amygdaloid kindled seizure in rats. Jingyi Ma et al. demonstrated that electrical kindling of the NAc resulted in convulsive seizure on animal models of psychosis (Ma and Leung, 2016). Zhou et al. showed that high frequency stimulation of the shell of the NAc significantly prolonged the latency to develop seizures, suppressed the severity of seizures, and reduced the second stage and total duration of seizures using pilocarpine-induced rodent models. These findings imply a protective role of NAc shell stimulation against seizures (Zhou Chenfei et al., 2014). Moreover, some recent clinical studies provided initial evidence for the safety and feasibility of chronic electrical stimulation of the NAc in patients with intractable partial epilepsy, as indicated by largely unchanged neurocognitive function and psychiatric comorbidity (Kowski et al., 2015; Schmitt et al., 2014). Peng et al. (2014) reported the first evidence of structural abnormalities in the nucleus accumbens along with other subcortical gray matter in patients with MRI-negative extemporal lobe cortical epilepsy. These findings, together with our

results, strongly support the role of the NAc shell in epileptogenesis from distinct perspectives.

Previous studies suggested that left TLE patients show a more distributed, bilateral pattern of structural changes compared to right TLE patients (Bonilha et al., 2007, 2010; Miro et al., 2015). In accordance with this, our left TLE patients showed bilateral NAc shell damage compared with the control group. However, contrary to our expectations, the right mTLE patients showed decreased FA and increased RD only in the left shell portion rather than the right shell portion. It is widely accepted that the left hemisphere is more vulnerable than the right and has a more prolonged network maturation and a distinct vulnerability due to perinatal vascular asymmetry (Besson et al., 2014; Miro et al., 2015). This may partly explain why the damage was observed in the left shell of the NAc rather than the right shell. Moreover, unlike the hippocampus and amygdala, the NAc was thought to be a way station or modulatory center in seizure transmission rather than the seizure focus (Löscher et al., 1996; Lothman et al., 1985; Pereira de Vasconcelos et al., 1999). Therefore, it seems reasonable that structural abnormalities were only observed in the contralateral shell portion in right TLE patients. Another compelling assumption that might explain the greater impairment of the left NAc shell in right mTLE patients is related to the biased interhemispheric connections that emerge from the temporal lobe toward contralateral temporal or frontal regions (Eross et al., 2009). The contralateral NAc shell abnormalities we found in the right mTLE patients give support to its role in interhemispheric seizure propagation and encourage future research about the specific connection alterations in each NAc subdivision in mTLE patients.

4.3 | Connectivity patterns of each NAc subdivision in healthy controls

Based on the group-averaged core and shell, we elucidated the anatomical connectivity patterns of the human NAc at the subregional level and demonstrated relatively distinct structural connectivity of each NAc subregion, without significant difference in hemispheres main effect. The preferential structural connectivity of core with caudate, FP, and THAL and for shell with AMYG, OFC, parahippocampus, putamen, SCC, and TP were in complete accordance with the reported differential afferent and efferent connections of the NAc subdivisions in the rat, monkey and postmortem human brain (Basar et al., 2010; Haber, 2011; Haber and Knutson, 2010).

However, this connectivity pattern is varied in some previous studies (Baliki et al., 2013; Lucas-Neto et al., 2015). Baliki et al. used diffusion tractography to subdivide the right NAc into lateral-rostral (putative core, pcore) and medial-caudal (putative shell, pshell) subdivisions in healthy humans and demonstrated a preferential structural connectivity of core with BG and OFC, and shell with AMYG. Lucas-Neto et al. performed in vivo delineation and segmentation of human NAc, observed a preferential connectivity of the core to the frontal pole and orbitofrontal cortex and of the shell with the anterior cingulate, amygdala, and temporal pole. This discrepancy may relate to the participants studied or different methodological approaches. Nevertheless, the preferential structural connectivity of core with caudate, FP, and THAL, and for shell with AMYG, OFC, parahippocampus, putamen, SCC, and TP we found may conform more to previously reported differential inputs and outputs of the NAc subdivisions (Basar et al., 2010; Feja et al., 2014; Salgado and Kaplitt, 2015).

4.4 | Connection abnormalities of each NAc subdivision in left and right mTLE patients

In general, more extensive and intense connection abnormalities, although not all of them significant, were observed in NAc shell portions in mTLE patients, which may also suggest that the accumbens shell is implicated in seizure propagation.

Left and right mTLE patients exhibited distinct connectivity patterns in both core and shell portions. We also found a more distributed, bilateral pattern of structural connectivity changes in left TLE patients than in right TLE patients. Such distinct network pathology agrees with several previous studies (Ahmadi et al., 2009; Besson et al., 2014; Bonilha et al., 2007; Miro et al., 2015).

The results of decreased relative connectivity in the left HIP-shell and THAL-shell in left mTLE patients suggest a loss in microstructural connections due to neuronal activation related to seizures. Both the ipsilateral hippocampus and thalamus have been implicated in various stages of mesial temporal lobe seizure evolution (Bartolomei, Chauvel, & Wendling, 2008; Bartolomei, Wendling, Bellanger, Regis, & Chauvel, 2001; Bertram, 2013). The increased connectivity in the ACC-shell, OFC-shell, PCG-shell, and SCC-shell perhaps represents aberrant connections which composing the hyperexcitable circuits that propagate and maintain seizures, which suggests that the NAc shell serves as a way station for seizure transmission from the mesial temporal lobe to the frontal lobe.

In accordance with the loss in the left NAc shell mentioned above, the loss in connections found in the left FP-shell pathway in right TLE patients supports its role of trans-hemispheric transmission in epileptic seizures. However, we only analyzed the probabilistic connections between each NAc subregion and sixteen predefined target regions in the ipsilateral hemisphere in this study. The specific trans-hemispheric circuits involved in TLE seizure evolution and the role of the NAc in trans-hemispheric transmission need to be verified in future work.

It is noteworthy that increased subcallosal cortex (SCC)–shell connectivities were significant both in left and right TLE patients. As an important hub that is widely connected with the cingulate, hippocampus, amygdala, orbitofrontal cortex and nucleus accumbens, the SCC has received considerable interest in recent years as a target for neuromodulation in patients with neuropsychiatric disorders (Gutman, Holtzheimer, Behrens, Johansen-Berg, & Mayberg, 2009; Hamani et al., 2009; Lujan et al., 2013; Riva-Posse et al., 2014; Vergani et al., 2016). Nevertheless, to the best of our knowledge, few reports have proposed that the SCC is implicated in seizure evolution. The increased connectivity in the SCC-shell tract in both left and right TLE patients may be related to some psychiatric comorbidities in temporal lobe epilepsy, which should be verified in future studies.

4.5 | Microstructural abnormalities in group-averaged white matter tracts of each NAc subdivision in TLE patients

Left mTLE patients presented with bilateral and extensive FA changes while the changes in right mTLE patients were restricted to the ipsilateral hemisphere, which was similar to the changes in structural connectivity patterns, although the changes in diffusion parameters of group-level common tract did not match well with the relative connectivity abnormalities in TLE patients. This finding may be due to the limited number of samples and encourages the performance of future studies. However, the MD changes did not show this tendency in both left and right TLE patients. More extensive damage was present in the ipsilateral tracts of left TLE patients, and the contralateral hemisphere in left TLE patients and bilateral tracts in right TLE patients exhibited restricted damage.

The combination of increased connectivity and reduced FA in SCC-shell and OFC-shell tracts is particularly striking and has not been reported in TLE patients before. The connectivity measure tests the number of connections that go from one point to another, whereas the FA value is thought to represent the structural integrity of those fibers (Concha, Livy, Beaulieu, Wheatley, & Gross, 2010; Shott, Pryor, Yang, & Frank, 2016). Previously, increased connectivity with reduced FA has been described, for instance, in patients with Alzheimer's disease and in recovered anorexia nervosa patients (Shott et al., 2016), which demonstrates the hypothesis of compensatory fiber growth. Such neuronal fiber loss and paradoxical increase in structural connectivity in mTLE patients has been reported by Bonilha et al. (2012), who demonstrated a regional decrease in the absolute connectivity among limbic regions in MTLE accompanied by an increase in the average limbic network clustering coefficient. Furthermore, the combination of greater connectivity and less fiber integrity that we found directly corroborates and supports the hypothesis that seizure induced neuronal loss and axonal damage may lead to the development of aberrant connections and eventually result in structural network reorganization, thereby facilitating epileptogenicity and recurrent seizures (Spencer, 2002).

5 | LIMITATIONS

Several limitations in this study need to be addressed. First, the core and shell portions were identified by location and shape as described in previous anatomical studies and as demonstrated in additional structural connectivity studies; however, there is an absence of verification by in vivo cytoarchitectural correspondence. Notwithstanding, we applied a new and more precise method to guide NAc shell stereotactic target localization in individual TLE patients. Second, as accumbens are tiny regions in the human brain, their segmentation and registration may not be sufficiently accurate, which could result in the spatial discontinuity of the clustered subregions. We did not place any spatial constraints on our parcellation scheme, which may also have induced discontinuous voxels in parcellation results (Eickhoff et al., 2015). We need to take spatial constraints into consideration in future work. Third, the traditional DTI method is not ideal for the accurate characterization of fiber directions (Jones, Knösche, & Turner, 2013). More plausible methods should be developed and used to parcellate human brain regions in vivo, such as parcellation based on the orientation distribution functions derived from the high angular resolution diffusion imaging, or even diffusion spectrum imaging data, and based on both connection profiles and tissue heterogeneity derived from diffusional kurtosis imaging. To validate the reproducibility of DTI connectivity-based parcellation method, we also conducted our parcellation scheme. However, we only performed the scan twice on one healthy subject and conducted our parcellation scheme on left NAc. Furthermore, the reproducibility of our parcellation scheme need to be investigated with a larger sample size in our future work.

6 | CONCLUSION

In summary, for a neurosurgical application, we parceled the nucleus accumbens into core and shell portions using DTI probabilistic tractography in individual mTLE patients and controls. The exact stereotactic anatomy of the core and shell portion of the NAc will help neurosurgeons to perform NAc shell deep brain stimulation (DBS) to suppress seizure propagation. Our results revealed that significant structural abnormalities and more extensive connection alterations mainly existed within the NAc shell portion, which may provide anatomical evidence in support of the role of the NAc shell in epileptogenesis. The neuronal fiber loss and paradoxical increased connectivity in the SCC-shell and OFC-shell tracts in mTLE patients may suggest the regeneration of aberrant connections, a compensatory and repair process ascribed to recurrent seizures that constitutes a characteristic change in the epileptic structural network.

ACKNOWLEDGMENTS

This work was partly funded by the National Key Research and Development Program of China (Grant number: 2016YFC0107104) and the Science and Technology Planning Project of Guangdong Province, China (Grant number: 2015B010131011). The authors express their appreciation to their patients and volunteers for participating in this study.

ORCID

Xixi Zhao http://orcid.org/0000-0002-5316-4629
Qianjin Feng http://orcid.org/0000-0001-8647-0596

REFERENCES

Ahmadi, M. E., Hagler, D. J., Jr., McDonald, C. R., Tecoma, E. S., Iragui, V. J., Dale, A. M., & Halgren, E. (2009). Side matters: diffusion tensor imaging tractography in left and right temporal lobe epilepsy. *AJNR American Journal of Neuroradiology*, *30*, 1740–1747.

Baliki, M. N., Mansour, A., Baria, A. T., Huang, L., Berger, S. E., Fields, H. L., & Apkarian, A. V. (2013). Parceling human accumbens into putative core and shell dissociates encoding of values for reward and pain. *Journal of Neuroscience*, *33*, 16383–16393.

Barron, D. S., Tandon, N., Lancaster, J. L., & Fox, P. T. (2014). Thalamic structural connectivity in medial temporal lobe epilepsy. *Epilepsia*, *55*, e50–e55.

Bartolomei, F., Chauvel, P., & Wendling, F. (2008). Epileptogenicity of brain structures in human temporal lobe epilepsy: a quantified study from intracerebral EEG. *Brain: A Journal of Neurology*, *131*, 1818–1830.

Bartolomei, F., Wendling, F., Bellanger, J. J., Regis, J., & Chauvel, P. (2001). Neural networks involving the medial temporal structures in temporal lobe epilepsy. *Clinical Neurophysiology*, *112*, 1746–1760.

Basar, K., Sesia, T., Groenewegen, H., Steinbusch, H. W., Visser-Vandewalle, V., & Temel, Y. (2010). Nucleus accumbens and impulsivity. *Progress in Neurobiology*, *92*, 533–557.

Berg, A. T., Berkovic, S. F., Brodie, M. J., Buchhalter, J., Cross, J. H., van Emde Boas, W., Engel, J., French, J., Glauser, T. A., Mathern, G. W., Moshe, S. L., Nordli, D., Plouin, P., Scheffer, I. E. (2010). Revised terminology and concepts for organization of seizures and epilepsies: report of the ILAE Commission on Classification and Terminology, 2005–2009 *Epilepsia*, *51*, 676–685.

Bertram, E. H. (2013). Neuronal circuits in epilepsy: do they matter? *Experimental Neurology*, *244*, 67–74.

Besson, P., Dinkelacker, V., Valabregue, R., Thivard, L., Leclerc, X., Baulac, M., … Dupont, S. (2014). Structural connectivity differences in left and right temporal lobe epilepsy. *NeuroImage*, *100C*, 135–144.

Bewernick, B. H., Hurlemann, R., Matusch, A., Kayser, S., Grubert, C., Hadrysiewicz, B., … Schlaepfer, T. E. (2010). Nucleus accumbens deep brain stimulation decreases ratings of depression and anxiety in treatment-resistant depression. *Biological Psychiatry*, *67*, 110–116.

Boccardi, M., Bocchetta, M., Aronen, H. J., Repo-Tiihonen, E., Vaurio, O., Thompson, P. M., … Frisoni, G. B. (2013). Atypical nucleus accumbens morphology in psychopathy: another limbic piece in the puzzle. *International Journal of Law and Psychiatry*, *36*, 157–167.

Bonilha, L., Edwards, J. C., Kinsman, S. L., Morgan, P. S., Fridriksson, J., Rorden, C., … Halford, J. J. (2010). Extrahippocampal gray matter loss and hippocampal deafferentation in patients with temporal lobe epilepsy. *Epilepsia*, *51*, 519–528.

Bonilha, L., Nesland, T., Martz, G. U., Joseph, J. E., Spampinato, M. V., Edwards, J. C., & Tabesh, A. (2012). Medial temporal lobe epilepsy is associated with neuronal fibre loss and paradoxical increase in structural connectivity of limbic structures. *Journal of Neurology, Neurosurgery & Psychiatry*, *83*, 903–909.

Bonilha, L., Rorden, C., Halford, J. J., Eckert, M., Appenzeller, S., Cendes, F., & Li, L. M. (2007). Asymmetrical extra-hippocampal grey matter loss related to hippocampal atrophy in patients with medial temporal lobe epilepsy. *Journal of Neurology, Neurosurgery, and Psychiatry*, *78*, 286–294.

Chowdhury, R., Lambert, C., Dolan, R. J., & Duzel, E. (2013). Parcellation of the human substantia nigra based on anatomical connectivity to the striatum. *NeuroImage*, *81*, 191–198.

Concha, L., Livy, D. J., Beaulieu, C., Wheatley, B. M., & Gross, D. W. (2010). In vivo diffusion tensor imaging and histopathology of the fimbria-fornix in temporal lobe epilepsy. *Journal of Neuroscience*, *30*, 996–1002.

Eickhoff, S. B., Thirion, B., Varoquaux, G., & Bzdok, D. (2015). Connectivity-based parcellation: Critique and implications. *Human Brain Mapping*, *36*, 4771–4792.

Eross, L., Entz, L., Fabo, D., Jakus, R., Szucs, A., Rasonyi, G., … Halasz, P. (2009). Interhemispheric propagation of seizures in mesial temporal lobe epilepsy. *Ideggyogyaszati Szemle*, *62*, 319–325.

Feja, M., Hayn, L., & Koch, M. (2014). Nucleus accumbens core and shell inactivation differentially affects impulsive behaviours in rats. *Progress in Neuropsychopharmacology & Biological Psychiatry*, *54*, 31–42.

Francis, T. C., Chandra, R., Friend, D. M., Finkel, E., Dayrit, G., Miranda, J., … Lobo, M. K. (2015). Nucleus accumbens medium spiny neuron subtypes mediate depression-related outcomes to social defeat stress. *Biological Psychiatry*, *77*, 212–222.

Gutman, D. A., Holtzheimer, P. E., Behrens, T. E., Johansen-Berg, H., & Mayberg, H. S. (2009). A tractography analysis of two deep brain stimulation white matter targets for depression. *Biological Psychiatry*, *65*, 276–282.

Haber, S. N. (2011). Frontiers in neuroscience neuroanatomy of reward: A view from the ventral striatum. In: J.A. Gottfried (Ed.), *Neurobiology of sensation and reward*. Boca Raton, FL: CRC Press/Taylor & Francis Llc.

Haber, S. N., & Knutson, B. (2010). The reward circuit: linking primate anatomy and human imaging. *Neuropsychopharmacology*, *35*, 4–26.

Hamani, C., Mayberg, H., Snyder, B., Giacobbe, P., Kennedy, S., & Lozano, A. M. (2009). Deep brain stimulation of the subcallosal cingulate gyrus for depression: anatomical location of active contacts in clinical responders and a suggested guideline for targeting. *Journal of Neurosurgery*, *111*, 1209–1215.

Jones, D. K., Knösche, T. R., & Turner, R. (2013). White matter integrity, fiber count, and other fallacies: The do's and don'ts of diffusion MRI. *NeuroImage*, *73*, 239–254.

Kandratavicius, L., Lopes-Aguiar, C., Bueno-Júnior, L. S., Romcy-Pereira, R. N., Hallak, J. E. C., & Leite, J. P. (2012). Psychiatric comorbidities in temporal lobe epilepsy: Possible relationships between psychotic disorders and involvement of limbic circuits. *Revista Brasileira De Psiquiatria*, *34*, 454–466.

Klein, J. C., Behrens, T. E., Robson, M. D., Mackay, C. E., Higham, D. J., & Johansen-Berg, H. (2007). Connectivity-based parcellation of human cortex using diffusion MRI: Establishing reproducibility, validity and observer independence in BA 44/45 and SMA/pre-SMA. *NeuroImage*, *34*, 204–211.

Kowski, A. B., Voges, J., Heinze, H. J., Oltmanns, F., Holtkamp, M., & Schmitt, F. C. (2015). Nucleus accumbens stimulation in partial epilepsy–a randomized controlled case series. *Epilepsia*, *56*, e78–e82.

Löscher, W., Ebert, U., & Lehmann, H. (1996). Kindling induces a lasting, regionally selective increase of kynurenic acid in the nucleus accumbens. *Brain Research*, *725*, 252–256.

Li, N., Wang, J., Wang, X. L., Chang, C. W., Ge, S. N., Gao, L., … Gao, G. D. (2013). Nucleus accumbens surgery for addiction. *World Neurosurgery*, *80*, S28 e29–S19.

Liu, H., Qin, W., Li, W., Fan, L., Wang, J., Jiang, T., & Yu, C. (2013). Connectivity-based parcellation of the human frontal pole with diffusion tensor imaging. *Journal of Neuroscience*, *33*, 6782–6790.

Lothman, E., Hatlelid, J., & Zorumski, C. (1985). Functional mapping of limbic seizures originating in the hippocampus: a combined 2-deoxyglucose and electrophysiologic study. *Brain Research*, *360*, 92–100.

Lucas-Neto, L., Reimao, S., Oliveira, E., Rainha-Campos, A., Sousa, J., Nunes, R. G., … Campos, J. G. (2015). Advanced MR imaging of the human nucleus accumbens–Additional guiding tool for deep brain stimulation. *Neuromodulation*, *18*, 341–348.

Lujan, J. L., Chaturvedi, A., Choi, K. S., Holtzheimer, P. E., Gross, R. E., Mayberg, H. S., & McIntyre, C. C. (2013). Tractography-activation models applied to subcallosal cingulate deep brain stimulation. *Brain Stimulation*, *6*, 737–739.

Ma, J., Boyce, R., & Leung, L. S. (2010). Nucleus accumbens mu opioid receptors mediate immediate postictal decrease in locomotion after an amygdaloid kindled seizure in rats. *Epilepsy & Behavior*, *17*, 165–171.

Ma, J., & Leung, L. S. (2010). Kindled seizure in the prefrontal cortex activated behavioral hyperactivity and increase in accumbens gamma oscillations through the hippocampus. *Behavioural Brain Research*, *206*, 68–77.

Ma, J., & Leung, L. S. (2016). Dual effects of limbic seizures on psychosis-relevant behaviors shown by nucleus accumbens kindling in rats. *Brain Stimulation*, *9*, 762–769.

Mavridis, I., Boviatsis, E., & Anagnostopoulou, S. (2011). Anatomy of the human nucleus accumbens: a combined morphometric study. *Surgical and Radiologic Anatomy*, *33*, 405–414.

Miro, J., Gurtubay-Antolin, A., Ripolles, P., Sierpowska, J., Juncadella, M., Fuentemilla, L., … Rodriguez-Fornells, A. (2015). Interhemispheric microstructural connectivity in bitemporal lobe epilepsy with hippocampal sclerosis. *Cortex*, *67*, 106–121.

Muller, U. J., Voges, J., Steiner, J., Galazky, I., Heinze, H. J., Moller, M., … Kuhn, J. (2013). Deep brain stimulation of the nucleus accumbens for the treatment of addiction. *Annals of the New York Academy of Sciences*, *1282*, 119–128.

O'Donnell, P., & Grace, A. A. (1995). Synaptic interactions among excitatory afferents to nucleus accumbens neurons: hippocampal gating of prefrontal cortical input. *J Neurosci*, *15*, 3622–3639.

Parekh, M. B., Carney, P. R., Sepulveda, H., Norman, W., King, M., & Mareci, T. H. (2010). Early MR diffusion and relaxation changes in the parahippocampal gyrus precede the onset of spontaneous seizures in an animal model of chronic limbic epilepsy. *Experimental Neurology*, *224*, 258–270.

Peng, S. J., Harnod, T., Tsai, J. Z., Ker, M. D., Chiou, J. C., Chiueh, H., … Hsin, Y. L. (2014). Evaluation of subcortical grey matter abnormalities in patients with MRI-negative cortical epilepsy determined through structural and tensor magnetic resonance imaging. *BMC Neurology*, *14*, 104.

Pereira de Vasconcelos, A., Mazarati, A. M., Wasterlain, C. G., & Nehlig, A. (1999). Self-sustaining status epilepticus after a brief electrical stimulation of the perforant path: a 2-deoxyglucose study. *Brain Research*, *838*, 110–118.

Postuma, R. B., & Dagher, A. (2006). Basal ganglia functional connectivity based on a meta-analysis of 126 positron emission tomography and functional magnetic resonance imaging publications. *Cerebral Cortex*, *16*, 1508–1521.

Rigoard, P., Buffenoir, K., Jaafari, N., Giot, J. P., Houeto, J. L., Mertens, P., … Bataille, B. (2011). The accumbofrontal fasciculus in the human brain: a microsurgical anatomical study. *Neurosurgery*, *68*, 1102–1111; discussion 1111.

Riva-Posse, P., Choi, K. S., Holtzheimer, P. E., McIntyre, C. C., Gross, R. E., Chaturvedi, A., … Mayberg, H. S. (2014). Defining critical white matter pathways mediating successful subcallosal cingulate deep brain stimulation for treatment-resistant depression. *Biological Psychiatry*, *76*, 963–969.

Salgado, S., & Kaplitt, M. G. (2015). The nucleus accumbens: A comprehensive review. *Stereotactic and Functional Neurosurgery*, *93*, 75–93.

Saygin, Z. M., Osher, D. E., Augustinack, J., Fischl, B., & Gabrieli, J. D. (2011). Connectivity-based segmentation of human amygdala nuclei using probabilistic tractography. *NeuroImage*, *56*, 1353–1361.

Schmitt, F. C., Voges, J., Heinze, H. J., Zaehle, T., Holtkamp, M., & Kowski, A. B. (2014). Safety and feasibility of nucleus accumbens stimulation in five patients with epilepsy. *Journal of Neurology*, *261*, 1477–1484.

Scholl, E. A., Dudek, F. E., & Ekstrand, J. J. (2013). Neuronal degeneration is observed in multiple regions outside the hippocampus after lithium pilocarpine-induced status epilepticus in the immature rat. *Neuroscience*, *252*, 45–59.

Seehaus, A. K., Roebroeck, A., Chiry, O., Kim, D. S., Ronen, I., Bratzke, H., … Galuske, R. A. W. (2013). Histological validation of DW-MRI tractography in human postmortem tissue. *Cerebral Cortex*, *23*, 442–450.

Shott, M. E., Pryor, T. L., Yang, T. T., & Frank, G. K. (2016). Greater insula white matter fiber connectivity in women recovered from anorexia nervosa. *Neuropsychopharmacology*, *41*, 498–507.

Spencer, S. S. (2002). Neural networks in human epilepsy: evidence of and implications for treatment. *Epilepsia*, *43*, 219–227.

Sturm, V., Lenartz, D., Koulousakis, A., Treuer, H., Herholz, K., Klein, J. C., & Klosterkötter, J. (2003). The nucleus accumbens: a target for deep brain stimulation in obsessive–compulsive- and anxiety-disorders. *Journal of Chemical Neuroanatomy*, *26*, 293–299.

Tomassini, V., Jbabdi, S., Klein, J. C., Behrens, T. E. J., Pozzilli, C., Matthews, P. M., … Johansen-Berg, H. (2007). Diffusion-weighted imaging tractography-based parcellation of the human lateral premotor cortex identifies dorsal and ventral subregions with anatomical and functional specializations. *The Journal of Neuroscience*, *27*, 10259–10269.

Vergani, F., Martino, J., Morris, C., Attems, J., Ashkan, K., & Dell'acqua, F. (2016). Anatomic connections of the subgenual cingulate region. *Neurosurgery*, *79*, 465–472.

Voorn, P., Brady, L. S., Berendse, H. W., & Richfield, E. K. (1996). Densitometrical analysis of opioid receptor ligand binding in the human striatum–I. Distribution of mu opioid receptor defines shell and core of the ventral striatum. *Neuroscience*, *75*, 777–792.

Voorn, P., Brady, L. S., Schotte, A., Berendse, H. W., & Richfield, E. K. (1994). Evidence for two neurochemical divisions in the human nucleus accumbens. *The European Journal of Neuroscience*, *6*, 1913–1916.

Wang, H., Huang, Y., Coman, D., Munbodh, R., Dhaher, R., Zaveri, H. P., … Eid, T. (2017). Network evolution in mesial temporal lobe epilepsy revealed by diffusion tensor imaging. *Epilepsia*, *58*, 824–834.

Zhou Chenfei, W. K., Songtao, Q., Hui, O., Kaijun, Y., Botao, X., & Dan, Z. (2014). Effect of high frequency deep brain stimulation to nucleus accumben on lithium-pilocarpine seizures in acute phase rats. *Chinese Journal of Neurosurgery* (In Chinese).

SUPPORTING INFORMATION

Additional Supporting Information may be found online in the supporting information tab for this article.

How to cite this article: Zhao X, Yang R, Wang K, et al. Connectivity-based parcellation of the nucleus accumbens into core and shell portions for stereotactic target localization and alterations in each NAc subdivision in mTLE patients. *Hum Brain Mapp*. 2018;39:1232–1245. https://doi.org/10.1002/hbm.23912